

This item is likely protected under Title 17 of the U.S. Copyright Law. Unless on a Creative Commons license, for uses protected by Copyright Law, contact the copyright holder or the author.

Access to this work was provided by the University of Maryland, Baltimore County (UMBC) ScholarWorks@UMBC digital repository on the Maryland Shared Open Access (MD-SOAR) platform.

**Please provide feedback**

Please support the ScholarWorks@UMBC repository by emailing [scholarworks-group@umbc.edu](mailto:scholarworks-group@umbc.edu) and telling us what having access to this work means to you and why it's important to you. Thank you.

## A CLOSE LOOK AT THE STATE TRANSITIONS OF GALACTIC BLACK HOLE TRANSIENTS DURING OUTBURST DECAY

E. KALEMCI,<sup>1</sup> J. A. TOMSICK,<sup>2</sup> R. E. ROTHSCHILD,<sup>2</sup> K. POTTSCHMIDT,<sup>3,4</sup> AND P. KAARET<sup>5</sup>

Received 2003 June 25; accepted 2003 November 12

### ABSTRACT

We characterize the evolution of spectral and temporal properties of several Galactic black hole transients during outburst decay using the data from well-sampled *Rossi X-Ray Timing Explorer* Proportional Counter Array observations close to the transition to the low/hard state. We find several global patterns of evolution for spectral and temporal parameters before, during, and after the transition. We show that the changes in temporal properties (sudden increase or decrease in the rms amplitude of variability) are much sharper than the changes in the spectral properties, and it is much easier to identify a state transition with the temporal properties. The spectral index shows a drop 3–5 days before the transition for some of our sources. The ratio of the power-law flux to the total flux in the 3–25 keV band increases close to the transition, which may mean that the system must be dominated by the coronal emission for the transition to occur. We also show that the power-law flux shows a sharp change along with the temporal properties during the transitions, which may indicate a threshold transition volume for the corona. The evolution of the spectral and temporal properties after the transition is consistent with the idea that the inner accretion disk moves away from the black hole. Based on the evolution of spectral and temporal parameters and changes during the transitions, we discuss possible scenarios of how the transition is happening.

*Subject headings:* black hole physics — X-rays: stars

*On-line material:* machine-readable table

### 1. INTRODUCTION

X-ray observations of Galactic black holes (GBHs) indicate that they are found in several distinct spectral states (Tanaka & Lewin 1995; McClintock & Remillard 2003). These states are generally determined by the relative strength of two different emission components: soft blackbody-like radiation from an optically thick, geometrically thin accretion disk and a harder component showing a power-law spectrum believed to originate from Compton upscattering of soft seed photons from the disk by a hot electron corona. Often a relation between the X-ray luminosity of the source and spectral states also exists. When the soft component dominates the spectrum, the 2–10 keV luminosity is relatively high ( $\gtrsim 10^{37}$  ergs s<sup>−1</sup>), and therefore this state is called the “high/soft state” (HS). When the hard component dominates, then usually the 2–10 keV luminosity is low ( $\lesssim 10^{37}$  ergs s<sup>−1</sup>), and this state is called the “low/hard state” (LS). This dependence shows that the mass accretion rate plays an important role in determining the spectral states. These states also differ in terms of their short-term timing properties. The HS is often characterized by a lack of or very low level of variability, whereas the LS shows very strong variability ( $\sim 30\%$  rms in 0.04–4 Hz). Recently, changes in the radio properties have also been associated with the spectral states. In the LS, compact, optically thick jets are

observed (Fender et al. 2001). During state transitions optically thin outflows are detected (Corbel et al. 2001), and during the HS the radio emission is quenched (Fender et al. 2001). There are also cases for which both spectral components are present at comparable strength, characterized by parameters that are intermediate between those of the HS and the LS. For such a case, if the source flux is lower than the HS flux, the state is often called the “intermediate state” (IS), and if the flux is higher than the HS flux, it is called the “very high state” (VHS). We note that the classification of these states is not rigorously defined and is still an active topic of debate.

Most of the GBHs are observed during outbursts caused by a sudden, dramatic increase of the mass accretion rate onto the black hole. Figure 1 shows several examples of outburst light curves discussed in this paper (see Kalemci 2002 for all of the All-Sky Monitor light curves). Because of the dependence of spectral states on the mass accretion rate, a GBH transient often follows a specific sequence of spectral states. It is usually observed in the LS at the beginning of the outburst. As flux increases, it makes a transition to the HS or the VHS. As the source decays toward quiescence, a transition to the LS is usually observed. Some transients might follow a more complicated sequence of states, and some stay in the LS throughout the outburst. It is generally believed that the state transitions involve large restructuring of the accretion geometry of GBHs (Esin, McClintock, & Narayan 1997; Zdziarski et al. 2002). Therefore, analysis of these sources during state transitions may probe the dynamics of their accretion structure. Although the mass accretion rate is a very important parameter for determining the spectral states, it is unlikely that the states and transitions are solely determined by this parameter. Some sources show hysteresis of the transition luminosities (the luminosity of transition from LS to HS during the beginning of the outburst is much higher than the luminosity of the transition from HS to LS during the outburst

<sup>1</sup> Space Sciences Laboratory, 7 Gauss Way, University of California, Berkeley, CA 94720-7450.

<sup>2</sup> Center for Astrophysics and Space Sciences, Code 0424, University of California at San Diego, La Jolla, CA 92093-0424.

<sup>3</sup> Max-Planck-Institut für Extraterrestrische Physik, Giessenbachstrasse 1, 85748 Garching, Germany.

<sup>4</sup> *INTEGRAL* Science Data Centre, Chemin d’Écogia 16, 1290 Versoix, Switzerland.

<sup>5</sup> Harvard-Smithsonian Center for Astrophysics, 60 Garden Street, Cambridge, MA 02138.

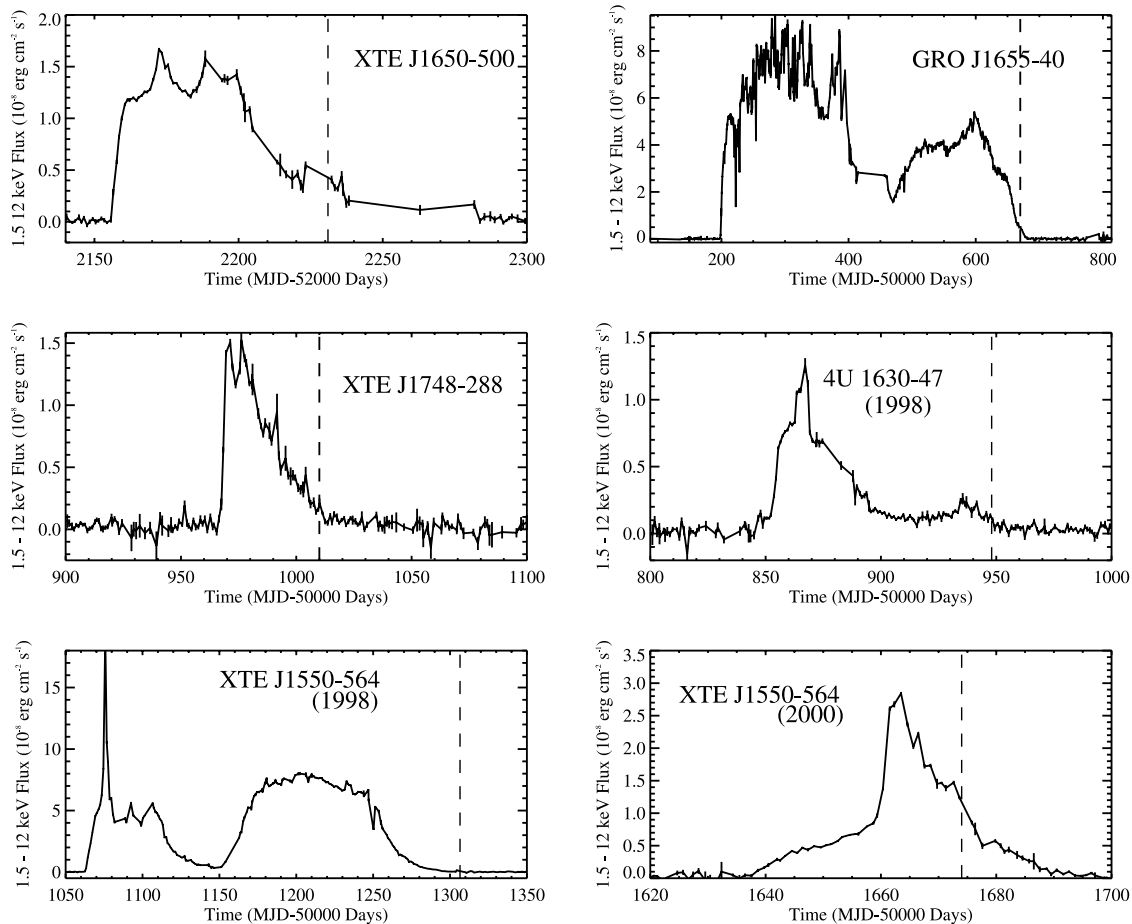


FIG. 1.—*RXTE* ASM light curves of six outbursts in the 1.5–12 keV band. The dashed lines represent the time of transition to the LS during outburst decay.

decay; Miyamoto et al. 1995; Nowak 2002; Maccarone & Coppi 2003), and for some sources, a second, independent parameter seems to be required to explain the complexity of transitions. It is not clear what this second parameter is. It might be the position of the inner edge of the accretion disk, but this position may not be completely independent from the mass accretion rate (e.g., Esin et al. 1997; Meyer, Liu, & Meyer-Hofmeister 2000). Based on the behavior of the 1998 outburst of XTE J1550–564, Homan et al. (2001) claimed that the second independent parameter may be the size of the corona. The transitions may also be a result of an overall change in the type and the geometry of the corona. Zdziarski et al. (2002) explain the different states in Cyg X-1 by the change of an accretion structure from one that consists of a hot inner accretion flow surrounded by an optically thick disk truncated far away from the minimum stable orbit in the LS to one that consists of flares and active regions above an accretion disk extending close to the minimum stable orbit in the so-called soft state. We note that for Cyg X-1, the soft state is more similar to the IS of GBH transients than the HS. According to the hybrid model of Coppi (1999), the state transitions can be explained by a change of size and electron energy distribution of the corona. In the LS, the inner part of the disk puffs up and becomes the hot corona, dominated by thermal electrons. Nonthermal electrons may also be present. In the HS, the edge of the cool accretion disk is close to the minimum stable orbit, and a small, nonthermal corona is also present. In this case, Compton scattering of disk photons by the nonthermal electrons is responsible for the steep power

law observed in the spectra of GBHs in the HS. It has also been claimed that this steep power-law component is a manifestation of Compton upscattering of disk photons by a converging inflow of material inside the last stable orbit (Laurent & Titarchuk 2001 and references therein). Then the transition might be related to the type of Comptonization: bulk motion in the HS versus thermal (or hybrid) in the LS.

The transition to the LS not only results in sharp changes in the X-ray spectrum, but also creates a physical environment that shows strong broadband variability and quasi-periodic oscillations (QPOs). The changes in the spectral parameters close to the state transition might provide important clues to the understanding of how this transition is occurring and what the driving force of the observed variability is. Our group has been observing GBH transients during outburst decays in X-rays with the *Rossi X-Ray Timing Explorer* (*RXTE*) and in radio. We have quantified the evolution before, during, and after the transition to the LS for various sources (Kalemci et al. 2001; Tomsick, Corbel, & Kaaret 2001; Kalemci et al. 2003; Tomsick et al. 2003). In § 3.1, we combine results of spectral and temporal analyses of the *RXTE* data from individual sources during outburst decay using our observations, as well as the archival data, and investigate the evolution of the spectral index ( $\Gamma$ ), the inner disk temperature ( $T_{\text{in}}$ ), the power-law flux, the disk-blackbody (diskbb) flux, and the power-law fraction (PLR, ratio of the power-law flux to the total flux in the 3–25 keV band) to obtain a global understanding of the physical environment before and during the state transition.

Another important topic is the evolution of spectral parameters after the state transition, which provides an understanding of the dynamics of the accretion systems in the LS. In addition to the spectral evolution, the evolution of the temporal parameters is another valuable tool in the LS. Thus, in § 3.2, we analyze the evolution of spectral and temporal parameters of GBH transients after the state transition. The temporal parameters we use are the characteristic frequencies of the Lorentzian components in the power–spectral density (PSD) fits and the rms amplitude of variability.

## 2. OBSERVATIONS AND ANALYSIS

We analyzed the *RXTE* PCA (Proportional Counter Array; see Bradt, Rothschild, & Swank 1993 for a description of *RXTE*) data from all GBH transients that have been observed between 1996 and 2001 that made a state transition during outburst decay. Eight sources in 11 outburst decays obey these source selection criteria. These sources and outburst years are XTE J1650–500 in 2001, GRO J1655–40 in 1996, XTE J1748–288 in 1998, XTE J1755–324 in 1997, GX 339–4 in 1998 (decayed in 1999), 4U 1630–47 in 1998, 1999, and 2001, XTE J1550–564 in 1998 and 2000, and XTE J1859+226 in 1999. Although XTE J1755–324 obeys the criteria, it has very poor coverage, and results from this source are not included in this work. This decreases the number of sources to seven, and the number of outbursts to 10. Note that XTE J1859+226 did not make a “traditional” transition to the LS; however, it showed timing noise for some observations during the decay (see Kalemci 2002 and references therein for the properties and observation times of each source).

For all of the spectral analysis, we fitted the data in the 3–25 keV band using the response matrix and the background model created using the standard FTOOLS (ver. 5.2) programs. We added a 1% systematic error to the spectra to account for uncertainties in the PCA response. We used a multicomponent spectral model consisting of a power-law, a multicolor disk blackbody (*diskbb* in XSPEC; Makishima et al. 1986), a broad absorption edge (*smedge* in XSPEC; Ebisawa et al. 1994), and interstellar absorption (*phabs* in XSPEC). This model has been commonly used for the spectral analysis of GBHs in the LS (Tomsick & Kaaret 2000; Sobczak et al. 2000). For all observations, the reduced  $\chi^2$  is between 0.5 and 1.5. For some observations, in order to reach acceptable  $\chi^2$  values, a Gaussian iron line feature was needed. However, the parameters of the iron line have not been used in the analysis. For some of the outbursts, we used published spectral fit parameters if the same model was applied for the fit (Tomsick & Kaaret 2000 for 4U 1630–47 in 1998 and Tomsick et al. 2001 for XTE J1550–564 in 2000). All PCA fluxes in this report are unabsorbed model fluxes to remove source-to-source variations due to different absorption column densities. The details of the spectral fit models and parameters for each source can be found in Kalemci (2002).

For the temporal analysis, we were as uniform as possible in terms of choosing energy bands, time resolution, and segmentation of light curves for all of our sources. However, since some of this work is based on the analysis of the archival data, we were limited to the choice of data modes by the principal investigator of the original proposal. For most of the observations we used the 2–26 keV energy band, a Nyquist frequency of 256 Hz, and 256 s light curve segments. Although there may be slight differences from source to source in terms of energy band and highest and lowest PSD

frequencies, these differences are not critical, since we look for trends rather than absolute values.

Historically, the PSD of GBHs during the LS has been modeled by a broken power law (or power laws with more than one break) plus narrow Lorentzians to fit the QPOs (Nowak et al. 1999; Tomsick & Kaaret 2000; Kalemci et al. 2001). However, recent papers successfully fit several GBH and neutron star PSDs with broad Lorentzians for the continuum and narrow Lorentzians for the QPOs (Belloni, Psaltis, & van der Klis 2002; van Straaten et al. 2002; Pottschmidt et al. 2003; Kalemci et al. 2003). Following this approach, we fitted all our PSDs with Lorentzians of the form

$$L_i(f) = \frac{R_i^2 \Delta_i}{2\pi \left\{ (f - f_i)^2 + [(1/2)\Delta_i]^2 \right\}}, \quad (1)$$

where subscript  $i$  denotes each Lorentzian component in the fit,  $R_i$  is the rms amplitude of the Lorentzian in the frequency band of  $-\infty$  to  $+\infty$ ,  $\Delta_i$  is the FWHM, and  $f_i$  is the resonance frequency. A useful quantity of the Lorentzian is the “peak frequency,” at which the Lorentzian contributes maximum power per logarithmic frequency interval:

$$\nu_i = f_i \left( \frac{\Delta_i^2}{4f_i^2} + 1 \right)^{1/2}. \quad (2)$$

Figure 2 shows an example LS power spectrum of XTE J1650–500 in the form of PSD  $\times$  frequency, along with broad and narrow Lorentzian fit components. In this figure, the Lorentzians peak at  $\nu_i$ , demonstrating the easy identification of characteristic frequencies as peak frequencies of Lorentzian components. Some of our observations contain a Lorentzian that is narrow (with quality value  $Q_i = f_i/\Delta_i > 2$ , as compared to  $Q < 1$  for broad Lorentzians), which we call a QPO. In this work, for each observation, the term “characteristic frequency” represents the resonance frequency of the fundamental QPO<sup>6</sup> if present, and otherwise the lowest peak frequency of the broad Lorentzian components in the PSD.<sup>7</sup> Note that since the QPO frequencies and the Lorentzian peak frequencies are all shown to be correlated (Belloni et al. 2002), it does not matter which one we use to characterize the evolution. The rms amplitudes are calculated over a frequency band from 0 to  $\infty$ .

Mostly because of our group’s monitoring program of GBHs with *RXTE* during outburst decay, we obtained very good coverage for three sources, in six different outbursts (1998, 1999, and 2001 outbursts of 4U 1630–47, 1998 and 2000 outbursts of XTE J1550–564, and the 2001 outburst of XTE J1650–500 with almost daily monitoring). GRO J1655–40 and GX 339–4 are excluded from the discussion in § 3.1 of the changes before and during the transition, since they have poor coverage ( $\geq 10$  days between observations). XTE J1748–288, with observations every  $\sim 5$  days, is included in the discussion of the evolution to the state transition, but is not included in the discussion of the changes during the transition. Results from these sources are included in the

<sup>6</sup> The peak frequency and the resonance frequency differ by  $< 3\%$  for QPOs with  $Q > 2$ .

<sup>7</sup> The lowest peak frequency is nearly equivalent to the “break frequency” if broken–power-law modeling is adopted; see Belloni et al. (2002) for a detailed discussion.

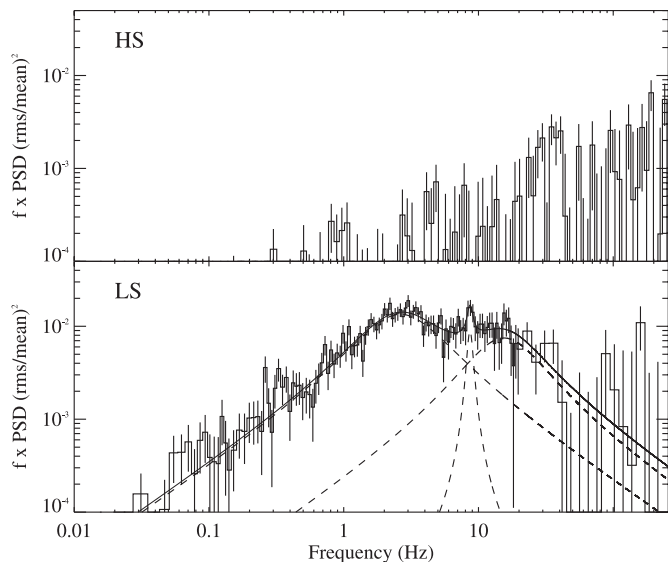


FIG. 2.—Power spectra of XTE J1650–500 in the HS (*top*) and in the LS (*bottom*). The PSD in the LS is fitted with one narrow and two broad Lorentzians. The HS observation has a  $2\sigma$  upper limit of 4% on the rms amplitude of variability, whereas the LS observation 2 days later has an rms amplitude of variability of  $12.43\% \pm 0.55\%$

discussion of the evolution after the transition, for which very good coverage is not necessary. All the data used in this report are available in the electronic edition of *Astrophysical Journal* as a machine-readable table. In Table 1, a portion of the online machine-readable table is printed for guidance regarding its form and content.

### 3. RESULTS

In this work, we define the state transition in terms of sharp changes in variability properties rather than sharp changes in spectral properties. All of our sources with good coverage showed sharp, distinct changes in terms of variability in less than 2 days, but this was not the case for the spectral properties. Most of the transitions occurred from the HS to LS, and for those cases the transition was marked by a very large increase in the total rms amplitude of variability as shown in Figure 3a. For most of the cases, the transition was from a featureless, Poisson noise-dominated PSD with only a few percent rms amplitude upper limit to a PSD showing well-defined broadband variability. In other words, the variability “appeared” on a timescale of a few days for these systems. Figure 2 represents this appearance of variability, as the observation in the HS (*top panel*, with  $<4\%$  rms upper limit variability) and the observation in the LS (*bottom panel*, with  $>12\%$  rms variability with well defined Lorentzian components and a QPO) in this figure are only 2 days apart. Since the HS PSD is often featureless and an amplitude of variability with little or no rms, it is not possible to discuss the evolution of characteristic frequencies before the transition for any of our sources except the 2000 outburst of XTE J1550–564, which showed a complex pattern. At this time, it was in the IS with rms amplitude variability of  $\sim 13\%$ . During the IS, it showed a QPO with constant frequency at  $\sim 9$  Hz. Then it showed a large drop in variability to an amplitude of  $\sim 7\%$ . We marked this change as the transition. Two days later, the rms amplitude of variability jumped again to levels of 15%. The morphology of the PSDs was different

during the IS, LS, and the time that the rms amplitude showed a drop (Kalemci 2002). Despite the complexity of some individual cases, it is possible to infer global patterns of evolution for different parameters before, during, and after the state transition.

#### 3.1. Changes in Spectral Properties that Lead to State Transitions

First, we characterize the changes in spectral properties before the state transition. The evolution of the photon spectral index ( $\Gamma$ ) and the inner disk temperature ( $T_{\text{in}}$ ) close to the transition are shown in Figures 3b and 3c, respectively. The evolution of the PLR, power-law flux, and diskbb flux are shown in Figure 4. In most sources,  $\Gamma$  (Fig. 3b) is approximately constant until 3–5 days before the timing transition, at which point it begins to decline. For some sources, there is a distinct drop in  $\Gamma$  at the beginning of the decline. Except for the 1998 outburst of XTE J1550–564,  $T_{\text{in}}$  (Fig. 3c) either decreases or stays constant before the transition. The power-law flux (Fig. 4b) shows a complex behavior (see also Fig. 5), and the diskbb-flux (Fig. 4c) decreases for the majority of the outbursts, or stays constant. The cumulative effect of the power-law and diskbb-flux evolution for the majority of the outbursts is an increasing PLR (Fig. 4a) before the transition.

We established that the transition occurs on a few days’ timescale for GBH transients. The change in variability properties (usually the appearance of variability) that defines the transition should be a response to the change of one or more spectral parameters. To understand which parameter drives the transitions and appearance of variability, we compared the two observations just before and after the transition (observations just before and after the dashed lines in Figs. 3 and 4). We specify that a spectral parameter is showing a sharp change during the transition if either the slope of the parameter as a function of time changes sign or the percentage change in the value of the parameter compared to the previous observation is at least 3 times that of the previous observation. With this definition, two parameters show a sharp change for the majority of the outbursts: the power-law flux (see Fig. 5) and the PLR.<sup>8</sup> The PLR is not an independent parameter, and in this case its increase is mostly driven by the increase in the power-law flux. For both the 1999 and the 2001 outbursts of 4U 1630–47, there is no sharp change in any of the spectral parameters between those two observations, yet one observation shows no variability and the next one shows variability. However, for both, the evolution of the power-law flux shows a change in the slope an observation earlier. The situation is more complicated for the 2000 outburst of XTE J1550–564. There is a large increase in the power-law flux and PLR during the transition, but this change corresponds to a decrease in the rms amplitude (Kalemci 2002).

Analysis of PCA data from GBH transient XTE J1859+226 during its outburst decay revealed interesting behavior in terms of variability and spectral evolution and provided another case for the relation between the power-law flux and variability. XTE J1859+226 did not show a traditional transition but showed variability for some of the observations during the decay. On a 1 day timescale, the power-law flux almost doubled and variability appeared, and when the

<sup>8</sup> GX 339–4, during its recent decay from the outburst, showed a large increase in the PLR, and by using this information, we were able to estimate when the transition would occur and schedule a successful *RXTE* observation to catch the beginning of the transition.

TABLE 1  
EVOLUTION OF SPECTRAL AND TEMPORAL PROPERTIES FOR GALACTIC BLACK HOLE TRANSIENTS CLOSE TO THE STATE TRANSITION

Observation	Date <sup>a</sup>	$\Gamma$	$T_{\text{in}}$	Power-Law Flux	Diskbb Flux	PLR	rms (%)	$\nu_1^b$	QPO Frequency <sup>c</sup>
XTE J1650–500									
1.....	52227.5	4.390 $\pm$ 0.343	0.484 $\pm$ 0.002	2.400 $\pm$ 0.264	5.255 $\pm$ 0.052	0.313 $\pm$ 0.030	<4 <sup>d</sup>	...	...
2.....	52228.1	4.026 $\pm$ 0.271	0.464 $\pm$ 0.007	2.211 $\pm$ 0.221	5.822 $\pm$ 0.058	0.275 $\pm$ 0.024	<4	...	...
3.....	52230.4	2.548 $\pm$ 0.140	0.487 $\pm$ 0.008	3.747 $\pm$ 0.337	5.080 $\pm$ 0.050	0.424 $\pm$ 0.036	<4	...	...
4 <sup>e</sup> .....	52231.0	2.415 $\pm$ 0.038	0.459 $\pm$ 0.004	4.524 $\pm$ 0.135	4.731 $\pm$ 0.047	0.488 $\pm$ 0.015	<4	...	...
5.....	52232.0	2.379 $\pm$ 0.019	0.489 $\pm$ 0.009	12.76 $\pm$ 0.127	4.171 $\pm$ 0.041	0.753 $\pm$ 0.009	12.42 $\pm$ 0.546	4.162 $\pm$ 0.498	...
6.....	52233.2	2.326 $\pm$ 0.023	0.443 $\pm$ 0.016	20.49 $\pm$ 0.204	2.221 $\pm$ 0.022	0.902 $\pm$ 0.010	19.01 $\pm$ 1.672	2.634 $\pm$ 0.202	8.734 $\pm$ 0.219
7.....	52234.5	2.093 $\pm$ 0.011	0.410 $\pm$ 0.035	30.62 $\pm$ 0.306	0.767 $\pm$ 0.030	0.975 $\pm$ 0.012	22.28 $\pm$ 1.992	1.274 $\pm$ 0.123	5.131 $\pm$ 0.090
8.....	52235.1	2.096 $\pm$ 0.009	0.355 $\pm$ 0.021	29.70 $\pm$ 0.297	0.569 $\pm$ 0.022	0.981 $\pm$ 0.012	23.04 $\pm$ 1.287	1.408 $\pm$ 0.089	5.440 $\pm$ 0.087
9.....	52236.1	2.001 $\pm$ 0.009	0.374 $\pm$ 0.033	28.70 $\pm$ 0.287	0.517 $\pm$ 0.036	0.982 $\pm$ 0.012	25.16 $\pm$ 1.614	0.881 $\pm$ 0.054	4.655 $\pm$ 0.072
10.....	52236.9	1.976 $\pm$ 0.007	0.321 $\pm$ 0.011	30.58 $\pm$ 0.305	0.271 $\pm$ 0.027	0.991 $\pm$ 0.012	24.75 $\pm$ 0.330	0.999 $\pm$ 0.028	3.799 $\pm$ 0.034
11.....	52237.9	1.961 $\pm$ 0.008	0.306 $\pm$ 0.006	29.59 $\pm$ 0.295	0.144 $\pm$ 0.014	0.995 $\pm$ 0.012	25.45 $\pm$ 2.449	0.974 $\pm$ 0.073	3.830 $\pm$ 0.077
XTE J1550–564, 1998									
1.....	1298.09	2.439 $\pm$ 0.134	0.415 $\pm$ 0.011	0.867 $\pm$ 0.065	0.547 $\pm$ 0.010	0.613 $\pm$ 0.048	<10	...	...
2.....	1299.34	2.688 $\pm$ 0.200	0.392 $\pm$ 0.011	0.567 $\pm$ 0.051	0.389 $\pm$ 0.007	0.593 $\pm$ 0.055	<10	...	...
3.....	1302.46	2.754 $\pm$ 0.278	0.394 $\pm$ 0.023	0.444 $\pm$ 0.066	0.219 $\pm$ 0.004	0.669 $\pm$ 0.106	<10	...	...
4.....	1303.39	2.635 $\pm$ 0.230	0.379 $\pm$ 0.027	0.532 $\pm$ 0.074	0.187 $\pm$ 0.005	0.739 $\pm$ 0.114	<10	...	...
5 <sup>e</sup> .....	1305.12	2.047 $\pm$ 0.141	0.464 $\pm$ 0.030	1.038 $\pm$ 0.072	0.228 $\pm$ 0.006	0.819 $\pm$ 0.066	<10	...	...
6.....	1307.32	1.968 $\pm$ 0.031	0.479 $\pm$ 0.104	3.746 $\pm$ 0.074	0.065 $\pm$ 0.005	0.982 $\pm$ 0.024	22.13 $\pm$ 1.590	1.175 $\pm$ 0.210	...
7.....	1309.72	1.739 $\pm$ 0.036	0.595 $\pm$ 0.084	2.377 $\pm$ 0.047	0.092 $\pm$ 0.007	0.962 $\pm$ 0.024	17.74 $\pm$ 0.600	0.551 $\pm$ 0.036	...
8.....	1311.52	1.785 $\pm$ 0.071	0.518 $\pm$ 0.073	1.216 $\pm$ 0.048	0.069 $\pm$ 0.006	0.946 $\pm$ 0.047	14.81 $\pm$ 1.590	0.144 $\pm$ 0.024	...
9.....	1313.32	1.773 $\pm$ 0.088	0.489 $\pm$ 0.058	0.861 $\pm$ 0.051	0.061 $\pm$ 0.006	0.933 $\pm$ 0.068	<8	...	...
10.....	1318.77	1.815 $\pm$ 0.132	0.455 $\pm$ 0.062	0.491 $\pm$ 0.039	0.045 $\pm$ 0.004	0.916 $\pm$ 0.089	<8	...	...

NOTES.—Table 1 is published in its entirety in the electronic edition of the *Astrophysical Journal*. A portion is shown here for guidance regarding its form and content.

<sup>a</sup> Date given in units of modified Julian date (MJD).

<sup>b</sup> Lowest peak frequency.

<sup>c</sup> Resonance frequency of the QPO if present.

<sup>d</sup> All upper limits are 2  $\sigma$ .

<sup>e</sup> The state transition happened between this observation and the next observation. The values in Figs. 3, 4, and 5 are normalized using parameters in this observation. Fig. 7 observations are normalized with respect to the next observation.

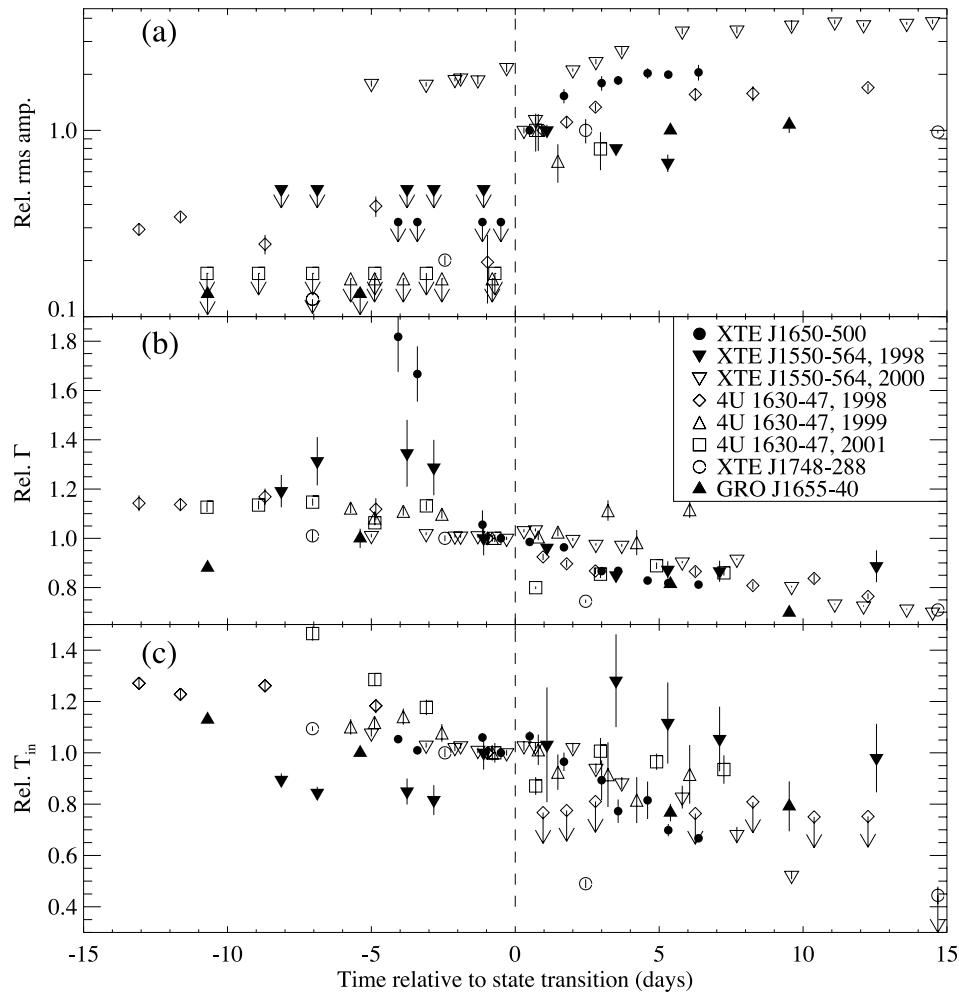


FIG. 3.—Evolution of (a) the rms amplitude of variability, (b) the spectral index, and (c) the inner disk temperature. The state transition is assumed to have happened exactly in between the observations closest to the sharp change observed in (a), and represented by a dashed line. For (a), the values for each source are normalized with respect to the value just after the state transition. For both (b) and (c), the values for each source are normalized with respect to the value just before the state transition. For some points, the  $1\sigma$  errors are smaller than the plot symbols. The upper limits are  $2\sigma$ .

power-law flux dropped below a threshold value, variability disappeared. Except for the PLR, which is tied to the power-law flux, no other spectral parameter showed a sharp change between observations that show variability and those that do not show variability for this source (Kalemci 2002).

### 3.1.1. Discussion of Transition Fluxes

It is important to get an idea of when the transition happens during the decay for effective monitoring of the sources with pointed instruments. Often the sources are not monitored frequently enough (i.e., once a day) with pointed observations, but the ASM measures the flux in three energy bands very frequently, which provides an opportunity to detect transitions without repointing the satellite. (See Fig. 1 for the ASM light curves of some of our sources.) The transition is often detected by a sudden increase in the hardness ratio 2 (HR2, the ratio of the 5–12 keV flux to the 1.5–3 keV flux). A few days just before and after the transition may manifest the most interesting behavior. A relationship between the peak flux and the transition flux (1.5–12 keV flux for the observation that shows variability) had been realized earlier (J. A. Tomsick 2002, private communication). We plot this relation for all of the outbursts that show a state transition in Figure 6. Except for the 1998 outburst of XTE J1550–564, which showed one of

the strongest flares in *RXTE* history, the transition flux increases with the peak flux. The Spearman rank order correlation coefficient for this data set (excluding the 1998 outburst of XTE J1550–564) is 0.90, pointing out a correlation. On the other hand, the linear correlation coefficient is 0.52, indicating a relation that is not strictly linear.

Some outbursts have the usual “fast rise–exponential decay” (FRED) shape (such as XTE J1748–288), and some have a very complicated shape (such as 4U 1630–47 in 2001). The complicated ones may show a plateau before the final decay (such as GRO J1655–40 and XTE J1550–564 in 2000; Fig. 1). For these sources, we also plotted the plateau ASM flux along with the peak flux. Replacing the peak flux by the plateau flux for these sources improves the linear correlation for the whole sample to  $r$  of 0.706. The linear correlation is not very strong, but it allows for an estimate of when the transition might happen, which is useful for planning observations to study the transition.

The recent work of Maccarone (2003) shows that the luminosities of transitions from the HS to the LS are tightly clustered for all the sources with good X-ray flux measurements at the time of the transition, good distance estimates, and good mass estimates for the compact star. This may indicate that the scatter in our peak flux–transition flux relation

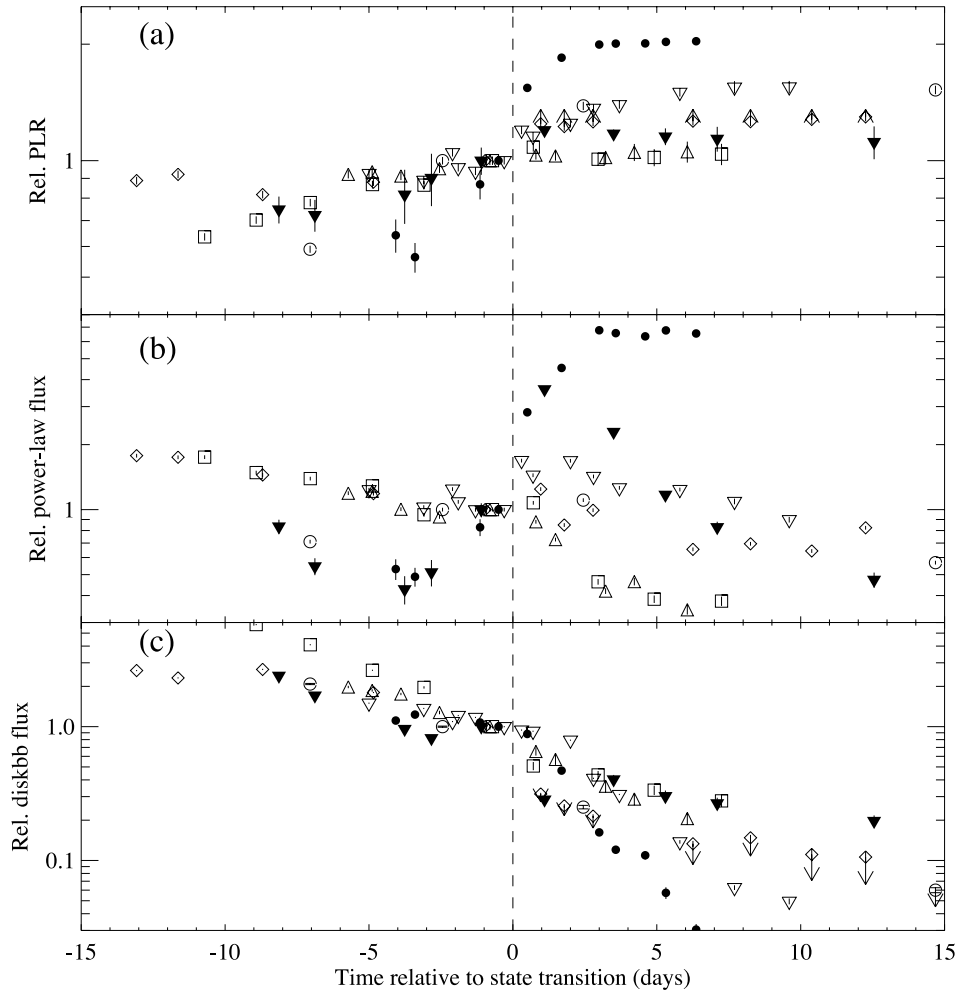


FIG. 4.—Evolution of (a) the PLR, (b) the power-law flux, and (c) the diskbb flux. The dashed line represents the time of transition. The values for each source are normalized with respect to the value just before the state transition. A legend is given in Fig. 3. For some points, the  $1\sigma$  errors are smaller than the plot symbols. The upper limits are  $2\sigma$ .

is mostly due to scatter in the peak luminosities, and the correlation may just reflect the distance differences (T. Maccarone 2002, private communication).

### 3.2. Evolution of Spectral and Temporal Parameters after the Transition

The evolution of spectral and temporal parameters after the transition is shown in Figures 3, 4, 5, and 7. For XTE J1650–500, GX 339–4 (not shown in Figs. 3, 4, and 5 because of poor coverage), 4U 1630–47 in 1998, and XTE J1550–564 in 2000,  $\Gamma$  decreases after the transition. For other outbursts, it is either constant or shows irregular behavior. The power-law flux decreases for all of the outbursts except XTE J1650–500 (see Figs. 4 and 5). For most cases, the diskbb flux and  $T_{\text{in}}$  either decrease or are unobservable after the transition. It is hard to constrain the evolution of  $T_{\text{in}}$  for the 1998 outburst of XTE J1550–564 and the 2001 outburst of 4U 1630–47. For all outbursts, the diskbb component is unobservable within 15 days of the state transition. For XTE J1650–500 and the 2000 outburst of XTE J1550–564, the PLR first increases and then stays constant. For all other outbursts, the PLR is very close to unity and does not vary.

The evolution of the characteristic frequencies after the transition is shown in Figure 7. Except for a single observation at the beginning of the 2000 outburst of XTE J1550–564, all

characteristic frequencies decrease after the transition. There are only two observations that show variability in the 1999 and 2001 outbursts of 4U 1630–47, and even for those cases, the later observations have smaller characteristic frequencies. The behavior of the rms amplitudes are more complicated (see Fig. 3a). The 1998 outbursts of XTE J1550–564 and XTE J1748–288 show a decreasing trend. The rms amplitudes for XTE J1650–500, the 2000 outburst of XTE J1550–564, and the 1998 outburst of 4U 1630–47 increase and level off. For GRO J1655–40, the rms amplitudes are consistent with being constant. For GX 339–4, on the other hand, the rms amplitude increases (Kalemci 2002).

## 4. DISCUSSION

### 4.1. State Transition and Appearance of Variability

First, we discuss possible reasons for the state transition and appearance of variability based on our results above. Suppose almost all of the variability we observe is due to the photons coming from the power-law component, presumably originating in the corona, and the disk photons are providing mostly Poisson noise. This idea is supported by the fact that very little or no variability is observed during the HS when the diskbb dominates, and strong variability is observed when the power-law component dominates in the LS. The anti-correlation between the diskbb flux and the rms amplitude

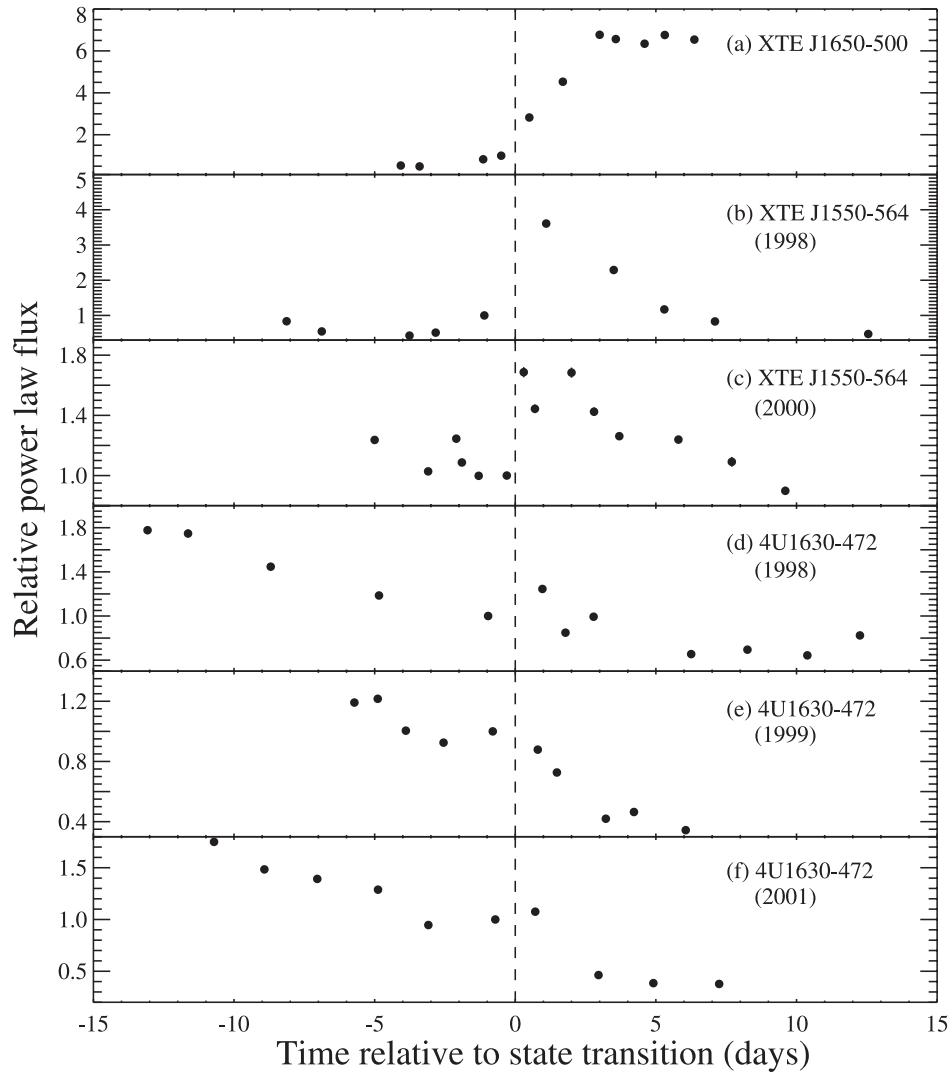


FIG. 5.—Evolution of the power-law flux before and after the transition. The dashed line indicates the time of the state transition. The values for each source are normalized with respect to the value just before the state transition. The  $1\sigma$  errors are smaller than the plot symbols

observed both in XTE J1650–500 (Kalemci et al. 2003) and the 2000 outburst of XTE J1550–564 (Kalemci et al. 2001) is also potentially consistent with this scenario. It is conceivable that the Poisson noise–dominated diskbb flux reduces the rms amplitudes of variability to unobservable levels. Then the PLR would be a good indicator of when the variability will be observed, since the higher the PLR, the lower the diskbb flux compared to the total flux. For all of our sources, no variability is observed if the  $\text{PLR} < 0.45$ . However, the value of the PLR cannot be the sole determinant of when the variability will be observed. For most of the sources the PLR has to be greater than 0.8 for the variability to appear, although it can be as low as 0.45 for XTE J1859+226 (Kalemci 2002). To test the argument that the diskbb flux might reduce the rms amplitudes to unobservable levels, we conducted very simple simulations. We added various levels of Poisson noise to the light curve of an observation of GRO J1655–40 taken on 1997 August 14 and compared the resultant PSD with the original PSD. We chose this observation since it has a complex structure and no diskbb flux, so all the emission is coming from the corona. The results are shown in Figure 8. Although this figure clearly shows that the rms amplitude of the PSD depends on the PLR, it also shows that even for a PLR of 0.3, the variability is

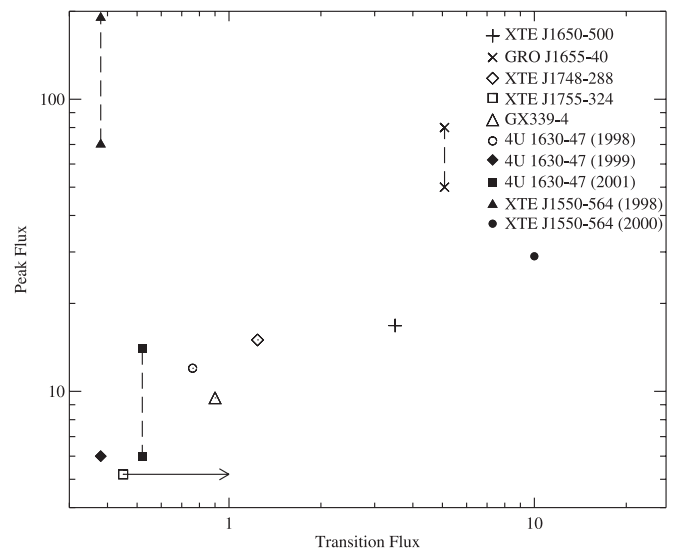


FIG. 6.—Peak flux vs. transition flux in the 1.5–12 keV band. Fluxes are in units of  $10^{-9}$  ergs  $\text{cm}^{-2}$   $\text{s}^{-1}$ . For the points connected with dashed lines, both peak fluxes and plateau fluxes are shown.

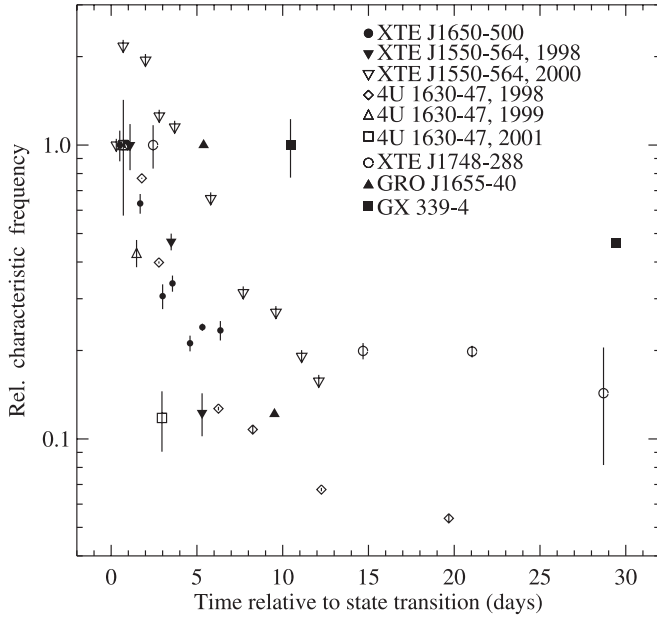


FIG. 7.—Evolution of the characteristic frequencies (the QPO resonance frequency for XTE J1550–564 in 2000, 4U 1630–47 in 1998 and 1999, and XTE J1748–288, lowest peak frequency of the broad Lorentzian components in the PSD for the remaining) after the state transition. For some points, the  $1\sigma$  errors are smaller than the plot symbols.

clearly observed. There is no large change in the PSD shape. Moreover, lack of diskbb emission *does not* guarantee broadband variability, even if a hard component exists. There is strong emission in the 6–15 keV band for most of the sources before the transition, and spectral analysis shows that only a few percent of the emission in this band is from the soft component. Nonetheless, although completely power law–dominated, these observations do not show variability. Note

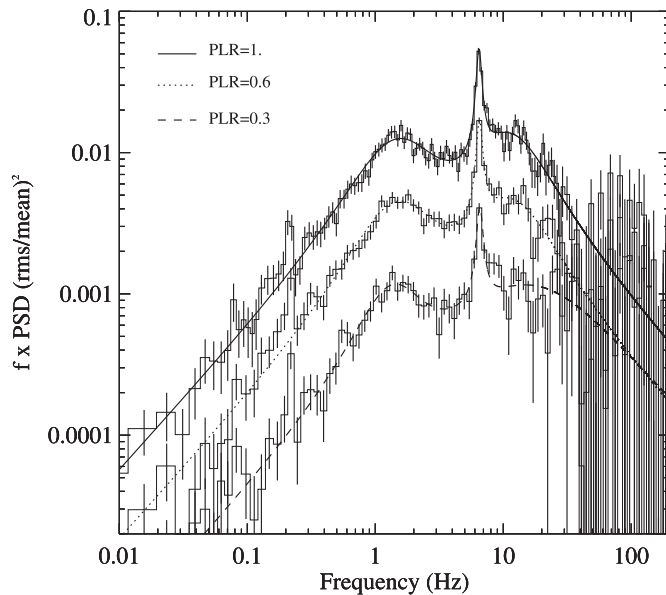


FIG. 8.—PSD of GRO J1655–40 during an observation in the LS, shown with the solid curve obtained by fitting the PSD with two broad Lorentzians and a QPO. The dotted and the dashed curves are fits to the PSDs when Poisson noise is added to the original light curve. The PSD under the dotted curve corresponds to a PLR of 0.6, and the PSD under the dashed curve corresponds to a PLR of 0.3.

that these simple simulations do not take into account the effects of strong disk emission on the corona. The two emission components are not independent of each other, because Compton cooling of the corona by the diskbb emission can affect the temperature and density structure of the corona. The amount of diskbb radiation cannot be ruled out as an important parameter in determining when the variability will be observed.

The power-law emission dominates the LS when the variability is observed, but its presence alone is not enough to create broadband variability. These findings suggest several possibilities for the presence of variability in the LS. The origin of the power-law component in the LS and the other states might be completely different. The passage from the IS to the LS (as observed for GX 339–4 and the 2000 outburst of XTE J1550–564) might be due to a change of the form of the corona from active regions above the accretion disk to an inner accretion flow (Zdziarski et al. 2002). The power-law component in the HS may be a result of Comptonization of disk photons by nonthermal electrons (Coppi 1999) or bulk-motion Comptonization (Laurent & Titarchuk 2001), whereas in the LS, it may be due to thermal Comptonization. However, if the form or the composition of the corona is changing during the transition, one would expect a sharp change not only in power-law flux, but also in  $\Gamma$ , especially if the change is from bulk-motion Comptonization to thermal Comptonization. There are two ways to increase the power-law flux, increasing the number of seed photons and/or increasing the area of the corona that intercepts the seed photons. It is unlikely that the number of seed photons is increasing: the corona is believed to be optically thin, and an increase in the soft flux should be observed (unless most photons have energies below the PCA range). Therefore, our findings are consistent with the idea that, during the transitions, the size of the corona increases to a threshold value for variability, which would be consistent with the idea of the second independent parameter determining the spectral states being the size of the Comptonizing region (Homan et al. 2001). The strongest support for this explanation comes from the behavior of XTE J1859+226. Variability appears for this source whenever the power-law flux is higher than a threshold value. No other spectral variable shows a significant change between observations with and without variability (Kalemci 2002). The only caveat to this scenario is the resemblance of the variability properties of XTE J1859+226 to the IS observations of GX 339–4 and the 2000 outburst of XTE J1550–564, rather than to the LS properties.

An increase in the power-law flux does not always correspond to the appearance of variability. The 2000 outburst of XTE J1550–564 behaved differently; the rms amplitude of variability decreased as the power-law flux increased sharply. But in a couple of days after the first transition, another transition occurred and strong variability that is usually associated with the LS appeared. The 1999 and the 2001 outbursts of 4U 1630–47 did not show a sharp change in any of the spectral properties at the transition (see Figs. 3 and 4), but both showed a change in the slope of the evolution of the power-law flux an observation earlier (see Fig. 5). This suggests the possibility that for some cases the appearance of variability (in the case of XTE J1550–564, variability associated with the LS) is delayed. The transition for these cases may be happening more slowly than that of other cases, and during the restructuring of the accretion geometry, the coherence could be lost for all timescales, and the timing signatures could be suppressed for a few days.

#### 4.2. Evolution of Spectral and Temporal Parameters

Two important observations about the transitions to the LS can be made by analyzing the evolution of spectral parameters before the transition. First, the PLR increases for the majority of the outbursts. The corona (again assumed to be the source of the power-law flux) must dominate for the transition to occur; the PLR is greater than 0.65 for all sources after the transition to the LS. The PLR was as low as 0.45 for XTE J1859+226 when the variability was observed, but it never made the transition to the canonical LS, and it returned to the HS when the PLR dropped (Kalemci 2002). Second, the spectral indexes for some of the sources show a step function-like decrease 3–5 days before the transition (see Fig. 3*b*). This can be interpreted as the time of spectral transition, which would indicate that the transition in timing properties lags the transition in spectral properties. Then the change in  $\Gamma$  may be a sign of the changing of form of the corona as discussed in § 4.1, and the lag between the change in  $\Gamma$  and the appearance of variability is the time it takes the corona to reach a threshold volume. However, some sources do not show any drop in  $\Gamma$  but still show a sharp change in temporal variability (Fig. 3*a*), making the transitions much easier to identify.

After the transition, the evolution of the inner disk temperature, the diskbb flux, the power-law index, and especially the characteristic frequencies of the variability are consistent with the idea of the inner disk retreat. In the basic formulation of Makishima et al. (1986), the optically thick disk has a temperature profile that decreases with increasing radius. Therefore, if the inner disk evaporates as part of the transition, it is expected that both  $T_{\text{in}}$  and the diskbb flux decrease. Most sources show a decrease in diskbb flux, and at least four sources show a decrease in  $T_{\text{in}}$ . The drop of spectral index may also be a sign of increasing inner disk radius. As the disk is closer to the black hole, its temperature and flux are higher, causing effective cooling of the corona, increasing the spectral index (Zdziarski et al. 2002). Four sources show a decreasing  $\Gamma$ . It is intuitively expected that the characteristic frequencies decrease as the inner disk radius increases. The dynamical timescale (the shortest timescale) in the accretion disk is shorter close to the black hole, and it is expected that higher frequency variability is created in this region. As the inner disk radius retreats (or the inner disk evaporates), the dynamical timescale (at the inner edge) increases, and therefore the characteristic frequencies in the PSD decrease. The exact relation between the characteristic frequencies and the dynamical timescales is not clear yet. All sources show a decreasing behavior in terms of characteristic frequencies, except for one observation. The overall evolution of both spectral and temporal properties therefore indicates that the inner edge of the accretion disk retreats as the system progresses in the LS, in accordance with the model of Esin et al. (1997). In the exceptional case, the QPO frequencies in the 2000 outburst of XTE J1550–564 first increased and then decreased after the transition (see Fig. 7). This behavior is consistent with the prediction of the “accretion ejection instability” QPO model (Tagger & Pellat 1999) if the inner accretion disk is close to the marginally stable orbit during this observation. This possibility is discussed in detail in Rodriguez et al. (2002) and Kalemci (2002).

The interpretation of the behavior of the rms amplitudes is more complex. We showed the relation between the PLR and the rms amplitudes earlier (see Fig. 8). The “Poissonic” nature of the disk component causes a decrease in the rms

amplitudes at lower energies because of the diskbb energy spectrum peaking at those energies. This might explain the increase and leveling of the rms amplitudes in XTE J1650–500 and the 2000 outburst of XTE J1550–564. Although the rms amplitudes seem to be decreasing after the transition for the 1998 outburst of XTE J1550–564, it might be a result of not constraining the high-frequency part of the PSD. The first observation requires two Lorentzians to fit and results in a high PSD amplitude, whereas for the remaining observations, the second Lorentzian, although statistically not required, cannot be excluded (Kalemci 2002). The fits are better for XTE J1748–288, the rms amplitude of which also shows a decrease. The interpretation of the rms amplitudes of XTE J1748–288 is complicated because of the high absorption column density. The Galactic ridge emission may also be affecting the rms amplitudes at low flux levels by supplying additional Poissonic emission. The rms amplitude of GX 339–4 increases after the transition, although there is no diskbb flux in the 3–25 keV band. Overall, there is no definite trend of evolution for the rms amplitudes after the transition.

#### 5. SUMMARY

An important goal of black hole binary research is to understand the accretion structure and nature of variability of these systems. This work addresses these goals by analyzing the X-ray temporal and spectral properties of a relatively large subset of GBHs during outburst decay. We characterize the evolution of spectral and temporal properties before and after the transitions and also work on the changes right at the transition to understand the appearance of broadband variability.

For this study, a total of seven *RXTE* sources in 10 outbursts are analyzed. Thanks to our group’s monitoring program, the coverage close to the transition is significantly improved, which for the first time allows us to determine the physical changes that drive the transitions in detail. The first problem we work on is the evolution of spectral parameters before the state transition and appearance of broadband variability at the state transition. We show that the changes in variability properties (a sudden increase or decrease in the rms amplitude of variability) are sharper than changes in spectral properties, and it is easier to identify a transition with the temporal properties. A change in the spectral index  $\Gamma$  is shown to be the precursor of the transition, with a decrease appearing 3–5 days before for most of our sources. We also show that the PLR increases close to the transition for all sources. The hard power-law component must dominate the spectrum for the transition to happen. Very frequent monitoring observations (approximately once a day) allow us to determine the power-law flux (and consequently the PLR) as the parameter that shows a sharp change during the transitions, which may indicate a threshold volume for the corona for the appearance of variability.

We also investigate the evolution after the state transition. For most of the cases, the  $T_{\text{in}}$  and the diskbb flux decrease after the transition, and they are unobservable with PCA within 15 days of the transition for all outbursts. The characteristic frequencies of all except one observation, the 2000 outburst of XTE J1550–564, decrease after the state transition. These spectral and temporal changes are consistent with the idea that the inner accretion disk retreats after the state transition. The rms amplitude of variability does not show any global trend with time after the transition, and its behavior is

consistent with the emission from the soft component having no or very little temporal signature.

E. K. acknowledges useful discussions with David Smith, Ali Alpar and Ünal Ertan. The majority of this work was done at the Center for Astrophysics and Space Sciences (CASS) at University of California, San Diego, as part of E. K.'s dissertation. E. K. acknowledges the support of the Astrophysics

Forum at Sabancı University, where a portion of this work was prepared, and also acknowledges partial support of TÜBİTAK. The authors would like to thank all scientists who contributed to the Tübingen Timing Tools. J. A. T. acknowledges partial support from NASA grant NAG5-13055. K. P. was supported by grant Sta 173/25-1 and Sta 173/25-3 of the Deutsche Forschungsgemeinschaft. P. K. acknowledges partial support from NASA grant NAG5-7405. This work was also supported by NASA contract NAS5-30720.

## REFERENCES

- Belloni, T., Psaltis, D., & van der Klis, M. 2002, *ApJ*, 572, 392  
 Bradt, H. V., Rothschild, R. E., & Swank, J. H. 1993, *A&AS*, 97, 355  
 Coppi, P. S. 1999, in *ASP Conf. Ser. 161, High Energy Processes in Accreting Black Holes*, ed. J. Poutanen & R. Svensson (San Francisco: ASP), 375  
 Corbel, S., et al. 2001, *ApJ*, 554, 43  
 Ebisawa, K., et al. 1994, *PASJ*, 46, 375  
 Esin, A. A., McClintock, J. E., & Narayan, R. 1997, *ApJ*, 489, 865  
 Fender, R. P., Hjellming, R. M., Tilanus, R. P. J., Pooley, G. G., Deane, J. R., Ogle, R. N., & Spencer, R. E. 2001, *MNRAS*, 322, L23  
 Homan, J., Wijnands, R., van der Klis, M., Belloni, T., van Paradijs, J., Klein-Wolt, M., Fender, R., & Méndez, M. 2001, *ApJS*, 132, 377  
 Kalemci, E. 2002, Ph.D. thesis, Univ. California, San Diego  
 Kalemci, E., Tomsick, J. A., Rothschild, R. E., Pottschmidt, K., Corbel, S., Wijnands, R., Miller, J. M., & Kaaret, P. 2003, *ApJ*, 586, 419  
 Kalemci, E., Tomsick, J. A., Rothschild, R. E., Pottschmidt, K., & Kaaret, P. 2001, *ApJ*, 563, 239  
 Laurent, P., & Titarchuk, L. 2001, *ApJ*, 562, L67  
 Maccarone, T. J. 2003, *A&A*, 409, 697  
 Maccarone, T. J., & Coppi, P. S. 2003, *MNRAS*, 338, 189  
 Makishima, K., Maejima, Y., Mitsuda, K., Bradt, H. V., Remillard, R. A., Tuohy, I. R., Hoshi, R., & Nakagawa, M. 1986, *ApJ*, 308, 635  
 McClintock, J. E., & Remillard, R. A. 2003, in *Compact Stellar X-Ray Sources*, ed. W. H. G. Lewin & M. van der Klis (Cambridge: Cambridge Univ. Press), in press (astro-ph/0306213)  
 Meyer, F., Liu, B. F., & Meyer-Hofmeister, E. 2000, *A&A*, 361, 175  
 Miyamoto, S., Kitamoto, S., Hayashida, K., & Egoshi, W. 1995, *ApJ*, 442, L13  
 Nowak, M. A., 2002, in *Proc. 4th Microquasars Workshop*, ed. Ph. Durouchoux, Y. Fuchs, & J. Rodriguez (Calcutta: Center Space Phys.), 3  
 Nowak, M. A., Vaughan, B. A., Wilms, J. J., Dove, J. B., & Begelman, M. C. 1999, *ApJ*, 510, 874  
 Pottschmidt, K., et al. 2003, *A&A*, 407, 1039  
 Rodriguez, J., Corbel, S., Kalemci, E., Tomsick, J. A., & Tagger, M. 2002, in *Proc. 4th Microquasars Workshop*, ed. Ph. Durouchoux, Y. Fuchs, & J. Rodriguez (Calcutta: Center Space Phys.), 64  
 Sobczak, G. J., McClintock, J. E., Remillard, R. A., Cui, W., Levine, A. M., Morgan, E. H., Orosz, J. A., & Bailyn, C. D. 2000, *ApJ*, 544, 993  
 Tagger, M., & Pellat, R. 1999, *A&A*, 349, 1003  
 Tanaka, Y., & Lewin, W. H. G. 1995, in *X-Ray Binaries*, ed. W. H. G. Lewin, J. Van Paradijs, & E. P. J. Van den Heuvel (Cambridge: Cambridge Univ. Press), 126  
 Tomsick, J. A., Corbel, S., & Kaaret, P. 2001, *ApJ*, 563, 229  
 Tomsick, J. A., & Kaaret, P. 2000, *ApJ*, 537, 448  
 Tomsick, J. A., Kalemci, E., Corbel, S., & Kaaret, P. 2003, *ApJ*, 592, 1100  
 van Straaten, S., van der Klis, M., di Salvo, T., & Belloni, T. 2002, *ApJ*, 568, 912  
 Zdziarski, A. A., Poutanen, J., Paciesas, W. S., & Wen, L. 2002, *ApJ*, 578, 357